

University of Nebraska - Lincoln

DigitalCommons@University of Nebraska - Lincoln

John R. Hardy Papers

Research Papers in Physics and Astronomy

2-5-1990

First-Principles Simulations of Ionic Molecular Solids: The Phase Transitions in K_2SeO_4

H. M. Lu

University of Nebraska - Lincoln

John R. Hardy

University of Nebraska - Lincoln

Follow this and additional works at: <https://digitalcommons.unl.edu/physicshardy>

 Part of the [Physics Commons](#)

Lu, H. M. and Hardy, John R., "First-Principles Simulations of Ionic Molecular Solids: The Phase Transitions in K_2SeO_4 " (1990). *John R. Hardy Papers*. 56.

<https://digitalcommons.unl.edu/physicshardy/56>

This Article is brought to you for free and open access by the Research Papers in Physics and Astronomy at DigitalCommons@University of Nebraska - Lincoln. It has been accepted for inclusion in John R. Hardy Papers by an authorized administrator of DigitalCommons@University of Nebraska - Lincoln.

First-Principles Simulations of Ionic Molecular Solids: The Phase Transitions in K_2SeO_4

H. M. Lu and J. R. Hardy

Department of Physics and Center for Electro-Optics, University of Nebraska-Lincoln, Lincoln, Nebraska 68588-0111

(Received 30 August 1989)

We present a new approach to first-principles simulations of the statics and dynamics of *ionic molecular* crystals. It is shown that the new method gives very realistic simulations of the phase transitions in K_2SeO_4 and that a double-well type of structure in the potential-energy surface is the driving mechanism of these phase transitions.

PACS numbers: 64.70.Kb, 64.70.Rh

First-principles simulations of complex ionic solids using *ab initio* pairwise interionic potentials have been highly successful in explaining melting,¹ superionicity,² and zone-boundary instabilities in halide perovskites.^{3,4} With the rigid-ion assumption and the short-range potentials for ion pairs computed from the free-ion closed-shell electron charge densities via the Gordon-Kim technique,⁵ this approach leads to accurate potential-energy surfaces for the systems under study.

However, when applied to study the phase transitions in Rb_2ZnCl_4 ,^{6,7} this method become inadequate. It was found that the short-range $Zn^{2+}-Cl^-$ potential for the $ZnCl_4^{2-}$ ion computed from the electron charge densities of the free Zn^{2+} and Cl^- ions was manifestly too hard and an overall reduction of this potential had to be adopted to give good agreement with the experimental Zn-Cl bond length. Also, some distortions of the $ZnCl_4^{2-}$ ion occurred, probably resulting from the combination of a lack of intramolecular bond-angle stiffness and full ionicity. This inadequacy of the method becomes even more obvious when it is used to treat K_2SeO_4 , where the required closed-shell electron-charge-density distribution would give selenium the unrealistically large ionicity of $6+$.

The basic shortcoming of this approach is the failure to treat the molecular ions as single entities. We believe that this need is quite general for a variety of systems which contain molecular ions, e.g., $ZnCl_4^{2-}$, SeO_4^{2-} , NO_2^- , SO_3^- , etc. Therefore the starting point in our new approach is to perform *ab initio* quantum chemistry calculations for the whole molecular ion, say SeO_4^{2-} in the case of K_2SeO_4 . The resultant electron-charge-density distribution accounts for possible charge transfer between the atoms within the group and thus leads to realistic Gordon-Kim potentials for intermolecular interactions. As for the intramolecular interactions, for which the simple Gordon-Kim model becomes invalid due to covalency, we use Taylor expansions of the molecular ions' total energy which can be constructed from the quantum chemistry calculations. These expansions are adequate owing to the stiffness of the intramolecular bonds.

We applied our new approach to simulation of the phase transitions in K_2SeO_4 , which, as the prototype of

the series of the A_2BX_4 compounds, has attracted extensive experimental and theoretical efforts.⁸ At room temperature it has an orthorhombic paraelectric phase (space group $Pnam$),⁹ with 4 formula units per unit cell, which changes to an incommensurate structure at 129.5 K (T_i). There follows a commensurate lock-in transition at 93 K (T_c) below which the crystal possesses an orthorhombic ferroelectric superstructure¹⁰ (space group $Pna2_1$) whose *a* axis is triple that of the room-temperature $Pnam$ phase.

We first performed a quantum chemistry structural optimization for an isolated SeO_4^{2-} ion. Thus the calculation did not include a crystal-field background, since over 90% of the contribution to the electric fields at the selenium and oxygen sites are from the other ions in the same SeO_4^{2-} group. The optimized SeO_4^{2-} forms a perfect tetrahedron with the Se-O bond length being 3.09 a.u., which is very close to the experimental average value of 3.07 a.u. in the $Pnam$ phase. Then the force constants at this optimized structure are calculated to give a harmonic expansion for the total energy of this ion. Since throughout, in the $Pnam$, incommensurate, and $Pna2_1$ phases, the SeO_4^{2-} ions stay as near-perfect tetrahedra, this expansion should give a satisfactory description of the Se-O and O-O interactions in the same SeO_4^{2-} ion.

We then calculated the electron charge density for the whole SeO_4^{2-} ion for the optimized structure and obtained charge densities for the individual Se and O atoms in the spirit of Mulliken population analysis. Pair potentials external to the SeO_4^{2-} units were then calculated via the Gordon-Kim technique using these charge densities and the free-ion charge density¹¹ for K^+ . These intermolecular pair potentials are much easier to employ for crystal simulations than complicated molecule-molecule potentials and we are not restricted to treating the selenate ions as rigid rotors. The quantum chemistry calculations were performed using the GAUSSIAN 86, program¹² and details of the calculations of the pair potentials will be given in future publications.¹³

With both the intramolecular and intermolecular interaction potentials determined we then performed a $Pnam$ -symmetry-restricted static relaxation for K_2SeO_4 , which should provide a rigorous test of theoretical

TABLE I. Prototypic atomic positions for K_2SeO_4 in the relaxed $Pnam$ structure. Experimental values (Ref. 9) are given in parentheses.

Prototype	x/a	y/b	z/c	Wyckoff designation
Se	0.2324 (0.2242)	0.4203 (0.4200)	$\frac{1}{4}$	4(c)
K(1)	0.1589 (0.1705)	0.0892 (0.0843)	$\frac{1}{4}$	4(c)
K(2)	0.9869 (0.9943)	0.6927 (0.7095)	$\frac{1}{4}$	4(c)
O(1)	0.3074 (0.2931)	0.3432 (0.3471)	0.0183 (0.0271)	8(d)
O(2)	0.3136 (0.3024)	0.5728 (0.5644)	$\frac{1}{4}$	4(c)
O(3)	0.0101 (0.0126)	0.4216 (0.4251)	$\frac{1}{4}$	4(c)

potential-energy surface. The relaxation is done with a lattice potential-energy minimization program developed in our group.^{7,13}

The lattice constants in the relaxed structure ($a=7.26$ Å, $b=9.86$ Å, $c=5.67$ Å) have an overall shortening of about 6% from the experimental values⁹ ($a=7.66$ Å, $b=10.47$ Å, $c=6.00$ Å), which is a rather general feature for large-unit-cell simulations using Gordon-Kim potentials. But the fractional basis vectors of the ions, as given in Table I, are very close to those in the experimental structure. The relaxed structure is plotted in Fig. 1(b), along with the experimental structure⁹ Fig. 1(a). For simplicity, only the projections of the ion positions parallel to the a axis are shown. As can be seen overall

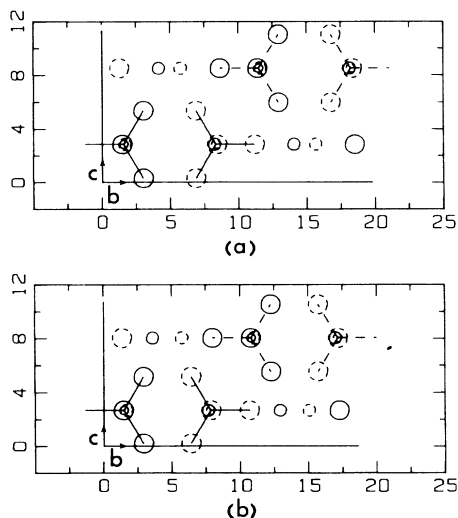


FIG. 1. Projections of ion positions parallel to the a axis in the (a) experimental and (b) simulated $Pnam$ structure of K_2SeO_4 . Bonds (straight lines) connect each selenium and the nearest four oxygen ions. The lattice constants are given in atomic units.

the simulation agrees very well with the experimental data.

Next we performed a static relaxation for the lower-temperature $Pna2_1$ superstructure of K_2SeO_4 , to provide a further test of the theoretical energy surfaces. In this phase the unit cell contains 12 formula units, in total 84 ions. Figure 2(a) gives the projections of the ion positions parallel the a axis in this phase, derived from experimental data at 80 K.¹⁰ Comparing Fig. 1(a) with Fig. 2(a), we see that the $Pna2_1$ superstructure is the result of a modulation along the a axis involving shifts of the K^+ ions and relative rotations of the SeO_4^{2-} ions, which are aligned in the $Pnam$ structure. Figure 2(b) gives the structure obtained by static relaxation with the $Pna2_1$ -symmetry restriction. Apart from a shortening of the lattice constants similar to that in the $Pnam$ phase, the relaxation again gives a close fit to the experimental structure. The basic modulation in the experimental structure is closely simulated, although the amplitudes are slightly different.

Given these excellent agreements with the experimental structure, we performed a nonconstrained molecular-dynamics (MD) "quench" for a $3a$ by $2b$ by $2c$ supercell containing 336 ions, using a constant (zero) pressure molecular-dynamics program also developed in our group.^{7,13} Starting from the $Pnam$ structure, the sample was first sufficiently relaxed to be as free of experimental information as possible and then cooled down in stages to $T=0$ K. We found that we could indeed reproduce the observed $Pnam$ - $Pna2_1$ phase transition by cooling in stages allowing an equilibration time of 2 ps at each

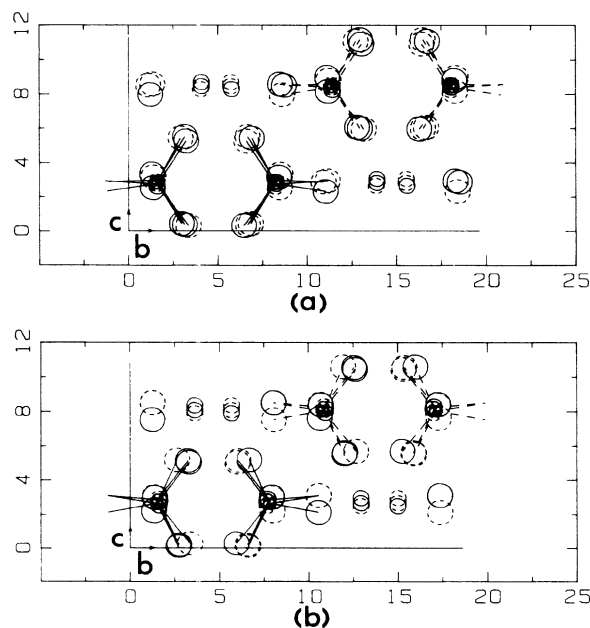


FIG. 2. Projections of ion positions parallel to the a axis in the (a) experimental and (b) simulated $Pna2_1$ superstructure of K_2SeO_4 .

stage. Figure 3 shows the **b-c** cross sections of the simulated structures at (a) $T=300$ K and (b) $T=57$ K, both averaged over 2 ps. In this figure, the average Se-O bonds are indicated by straight lines and the thermal motions of the ions are given by ellipsoids centered at the average ion positions. The structure in Fig. 3(a) is virtually the same as the experimental *Pnam* structure. The large (about 1 bohr) amplitudes of the thermal motions of some of the oxygen ions indicate that the crystal at this temperature is actually in a dynamically disordered state. This is in accord with a previous hypothesis made on the basis of the internal-mode Raman spectra.¹⁴ The structure in Fig. 3(b) is clearly the *Pna*2₁ structure given in Fig. 2(a). The positions of some of the ions appear slightly different, but again the basic modulation of the ions along the **a** axis agrees well with the experimental structure. In fact, when further cooled to $T=0$ K, this structure agrees closely with the theoretical *Pna*2₁ structure [Fig. 2(b)] both in structure and in potential energy.

In order to monitor more precisely the phase transition, we performed a CPU-intensive MD calculation for a **3a** by **2b** by **4c** supercell (672 ions) with 40-ps averaging time at each temperature, and then calculated the rms static deviation R of the Se-O bonds from their orientations in the *Pnam* phase as a convenient order parameter. The result is plotted in Fig. 4 together with the value of R for the experimental *Pna*2₁ structure at 80

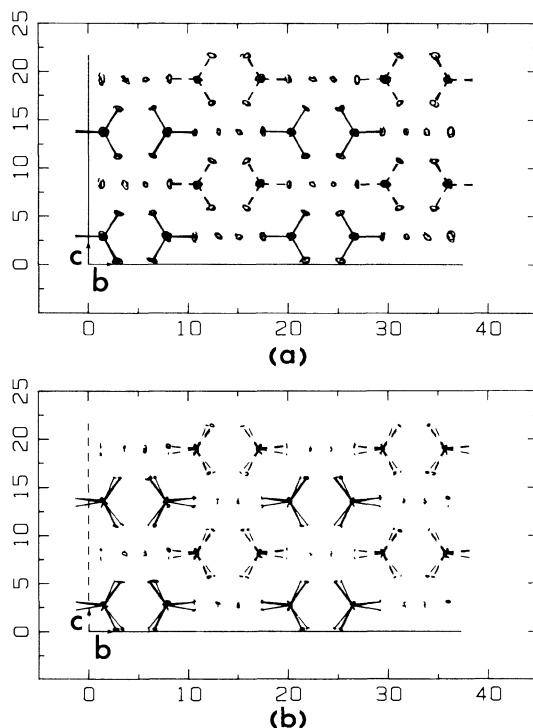


FIG. 3. Projections of the average ion positions in the structures at (a) $T=300$ K and (b) $T=57$ K obtained in the dynamics simulation for K_2SeO_4 . The ellipsoids indicate the thermal motions of the ions.

K.⁹ Figure 4 shows that the onset of the transition lies in the range 120–140 K, which corresponds closely to the incommensurate phase transition at $T_i=129.5$ K, and the transition is virtually complete at about the ferroelectric lock-in transition $T_c=93$ K. The behavior of the order parameter around 200 K was observed in several simulations; it is probably a dynamical, but slow, precursor to the main transition. To clarify this point would require a more extensive computation for an even larger number of ions, and this is beyond our computing resources.

The above excellent agreement with the experimental data leads us to conclude that we indeed have found a very realistic *ab initio* potential-energy surface of K_2SeO_4 and from it we have obtained a first-principles explanation for the driving mechanism of the phase transitions in K_2SeO_4 . From Fig. 2(b) we see that the modulation that changes the *Pnam* phase to the *Pna*2₁ superstructure is characterized by rotations of the selenate ions in two opposite directions away from their orientations in the *Pnam* structure. This suggests that the two rotated positions of the selenate ions may be equivalent in energy. This is indeed the case, as we found by explicit calculation for a single unit cell of 28 ions; both are 12.3 meV per formula unit lower than the *Pnam* structure. Since the *Pna*2₁ structure is 10.7 meV per formula unit lower in energy than the *Pnam* phase, these two structures are effectively degenerate for temperatures ~ 100 K and above. As a consequence when kT becomes less than ~ 10 –15 meV, and the structure transforms, the state selected will be that of higher entropy. Clearly, this is the *Pna*2₁ phase in which, for example, the SeO_4^{2-} ions have three rather than one possible orientation. Furthermore, for the *Pna*2₁ structure to transform to the single-cell, selenate-rotated, phase requires that at least one of the tetrahedra has to switch through the *Pnam* configuration. As the system is further cooled this becomes increasingly difficult, and when $kT \sim 1$ –2 meV (when the single cell phase would become preferred energetically), the transformation is frustrated by the ~ 10 -meV activation barrier, and the *Pna*2₁

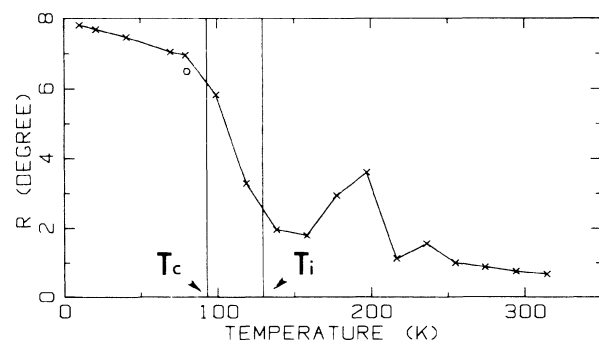


FIG. 4. Theoretical (\times) and experimental (\circ) order-parameter values as functions of temperature.

phase persists.

This work was supported by the U.S. Army Research Office. We should also like to acknowledge many helpful discussions with Dr. P. J. Edwardson and Dr. D. P. Billesbach.

¹L. L. Boyer, Phys. Rev. Lett. **42**, 584 (1979). A fuller account is given in Phys. Rev. B **23**, 3673 (1981).

²L. L. Boyer, Phys. Rev. Lett. **45**, 1858 (1980); **46**, 1172 (1981).

³L. L. Boyer and J. R. Hardy, Phys. Rev. B **24**, 2527 (1981).

⁴L. L. Boyer, J. Phys. C **17**, 1825 (1984).

⁵R. G. Gordon and Y. S. Kim, J. Chem. Phys. **56**, 3122 (1971).

⁶V. Katkanant, P. J. Edwardson, J. R. Hardy, and L. L. Boyer, Phys. Rev. Lett. **57**, 2033 (1986).

⁷P. J. Edwardson, V. Katkanant, J. R. Hardy, and L. L. Boyer, Phys. Rev. B **35**, 8470 (1987).

⁸See M. S. Haque and J. R. Hardy, Phys. Rev. B **21**, 245 (1980), and references therein.

⁹A. Kalman, J. S. Stephens, and D. W. J. Cruickshank, Acta Crystallogr. Sect. B **26**, 1451 (1970).

¹⁰N. Yamada, Y. Ono, and T. Ikeda, J. Phys. Soc. Jpn. **53**, 2565 (1984).

¹¹E. Clementi and C. Roetti, At. Data Nucl. Data Tables **14**, 177 (1974).

¹²M. J. Frisch *et al.*, GAUSSIAN 86 (Carnegie-Mellon Quantum Chemistry Publishing Unit, Pittsburgh, PA, 1984).

¹³H. M. Lu and J. R. Hardy (to be published).

¹⁴V. Katkanant, J. R. Hardy, and F. G. Ullman, Ferroelectrics **82**, 185 (1988).